SCIENTIFIC REPORTS

OPEN

Non-blocking modulation contributes to sodium channel inhibition by a covalently attached photoreactive riluzole analog

Peter Lukacs[1,6], Mátyás C. Földi[1,4], Luca Valánszki[1,4], Emilio Casanova [2,3], Beáta Biri-Kovács[4], László Nyitray[4], András Málnási-Csizmadia[4,5] & Arpad Mike[1,6]

Sodium channel inhibitor drugs decrease pathological hyperactivity in various diseases including pain syndromes, myotonia, arrhythmias, nerve injuries and epilepsies. Inhibiting pathological but not physiological activity, however, is a major challenge in drug development. Sodium channel inhibitors exert their effects by a dual action: they obstruct ion flow ("block"), and they alter the energetics of channel opening and closing ("modulation"). Ideal drugs would be modulators without blocking effect, because modulation is inherently activity-dependent, therefore selective for pathological hyperactivity. Can block and modulation be separated? It has been difficult to tell, because the effect of modulation is obscured by conformation-dependent association/dissociation of the drug. To eliminate dynamic association/dissociation, we used a photoreactive riluzole analog which could be covalently bound to the channel; and found, unexpectedly, that drug-bound channels could still conduct ions, although with modulated gating. The finding that non-blocking modulation is possible, may open a novel avenue for drug development because non-blocking modulators could be more specific in treating hyperactivity-linked diseases.

Voltage-gated sodium channels (VGSC) are essential components of electrical signal propagation in excitable tissues. Dysfunction of sodium channels may cause hyperexcitability, leading to several pathologies, including different pain syndromes, certain types of epilepsy, myotonia and arrhythmia. Hyperexcitability may ensue from modification of channel and pump functions following mechanical injury, ischemic injury or inflammation. Overexcitation is thought to be involved in several neurodegenerative and psychiatric diseases[1,2]. Inhibition of sodium channels may be an effective treatment for these conditions, however, non-selective inhibition could not be beneficial because of the vital role sodium channels play in neuronal and muscle function. Isoform selective sodium channel inhibitor drugs could be a solution for this problem, but due to a highly conserved drug-binding region[3], it has been difficult to develop isoform-selective drugs[4,5]. Fortunately, most sodium channel inhibitors exert a certain degree of functional selectivity, showing a definite preference for cells with abnormally high activity or a slightly depolarized membrane potential. In order to be able to find and develop drugs with high functional selectivity, it is essential to understand the mechanisms behind this phenomenon. Sodium channel inhibitors differ remarkably in their modes of action[6]: which conformations they prefer, at which conformations can they access their binding site, and what are the rates of association and dissociation. We also propose in this study that they might also differ in the way inhibition is effectuated: by channel block or by modulation.

Sodium channel inhibitors can exert their effect via two major mechanisms. Channel block means physical occlusion of the pore that prevents conduction sterically or electrostatically. Modulation, on the other hand, produces inhibition by energetically stabilizing one of the channel's native non-conducting conformations. This

[1]MTA-ELTE NAP B Opto-Neuropharmacology Group, Budapest, Hungary. [2]Department of Physiology, Center of Physiology and Pharmacology & Comprehensive Cancer Center (CCC), Medical University of Vienna, Vienna, Austria. [3]Ludwig Boltzmann Institute for Cancer Research (LBI-CR), Vienna, Austria. [4]Department of Biochemistry, Eötvös Loránd University, Budapest, Hungary. [5]MTA-ELTE Molecular Biophysics Research Group, Eötvös Loránd University, Budapest, Hungary. [6]Plant Protection Institute, Centre for Agricultural Research, Hungarian Academy of Sciences, Martonvásár, Hungary. Peter Lukacs and Mátyás C. Földi contributed equally to this work. Correspondence and requests for materials should be addressed to A.M. (email: arpadmike1@gmail.com)
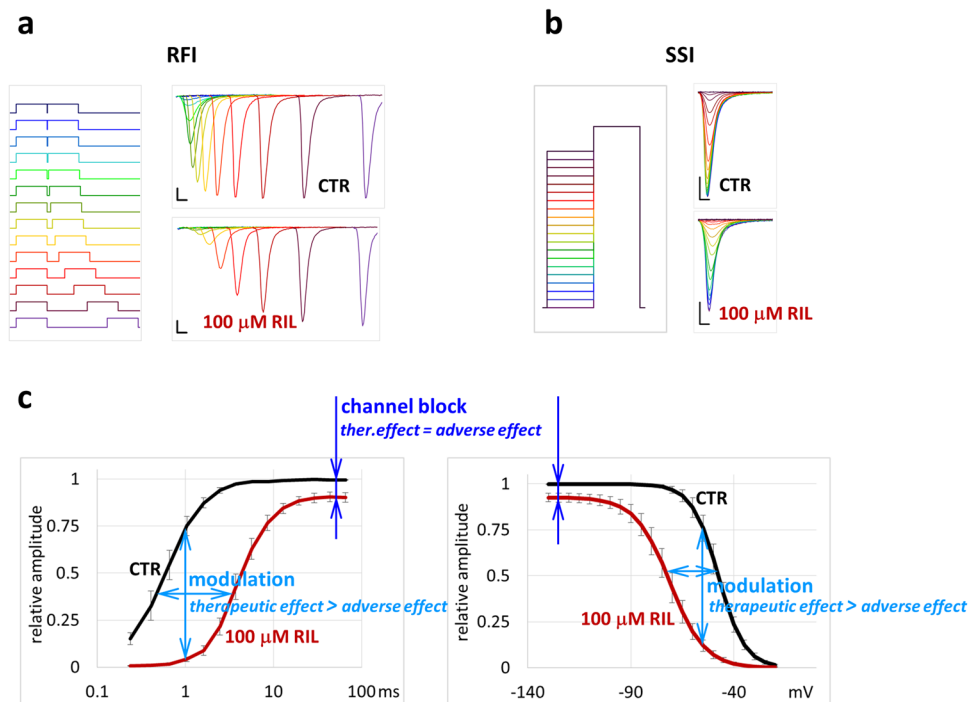
Figure 1. The extent of channel block and modulation can be assessed using **RFI** and **SSI** protocols. (**a**) Illustration of the first 22 ms of the **RFI** protocol. Left panel indicates the arrangement of 10 ms long depolarizing pulses (−130 to −10 mV), right panel illustrates currents evoked by the 2nd pulse in a cell in control solution and in the presence of riluzole, on linear time scale. Scale bars: 1 ms and 1 nA. (**b**) Illustration of the **SSI** protocol. Left panel shows the voltage protocol (10 ms pre-pulses from −130 to −20 mV in 5 mV increments, followed by a 10 ms test pulse to −10 mV). Right panel shows examples for currents evoked by the test pulse in control solution and in the presence of riluzole. (**c**) Assessment of channel block and modulation using the **RFI** (plotted on a logarithmic time scale) and **SSI** protocols. Amplitudes were normalized to the maximum amplitude of control; mean amplitudes were obtained as described in text. Resting channel block is observed when sufficient time has been spent at hyperpolarized membrane potential. The effect of modulation is seen by the shift of curves.

is typically inactivated conformation, a state assumed by the channel upon prolonged depolarization (either after opening or even without opening), which is essential in preventing overexcitation, and in making signal propagation by self-regenerating sodium channel activation. Common sodium channel inhibitor drugs are state-dependent: they produce a weaker inhibition at hyperpolarized membrane potentials, which is assumed to be due to channel block, and a much stronger inhibition at depolarized membrane potentials, which is thought to be due to a higher degree of channel block and, in addition, to modulation as well. The ability to modulate by stabilizing inactivated state also implies that the drug must have higher affinity to this conformation, according to the modulated receptor hypothesis[7,8]. Besides state-dependent affinity, state-dependent accessibility also contributes to the strong dependence of inhibition on membrane potential, as pointed out by the guarded receptor hypothesis[9]. The result of state-dependence is manifested in phenomena typical of sodium channel inhibitors: Besides reduced amplitude of sodium currents, the voltage dependence of availability is shifted towards hyperpolarized potentials, as measured in the widely used "steady-state inactivation" (**SSI**) protocol; and the recovery from the inactivated state is delayed, as measured in the "recovery from inactivation" (**RFI**) protocol (Fig. 1).

From the therapeutic point of view, conformational-state-dependent inhibition is more desirable than channel block, because while resting channel block equally affects healthy and diseased cells, state-dependent inhibition depends on the membrane potential and activity pattern of the cell, and therefore is selective for diseased cells.

In several pathological states such as traumatic injury, inflammation or ischemia, cells have a compromised ability to maintain the resting membrane potential. In addition, alterations in the expression level and function of various ion channels may develop, which often make the cell hyperexcitable. In the case of sodium channels these alterations typically involve enlarged or left-shifted window currents[10,11], and/or increased persistent current[12]. Inherited malfunction of channels (channelopathies) may also be the cause of hyperexcitability. Abnormally high firing rates and/or lower threshold for firing may lead to disorders such as types of myotonia, pain syndromes, epilepsies, and arrhythmias, and are involved in acute and chronic neurodegenerative diseases as well. An ideal sodium channel inhibitor, should prevent hyperexcitability, while not affecting normal excitability. For this reason, state-dependent inhibition is more desirable than resting channel block. For therapeutic purposes compounds should be screened for high state-dependence not high affinity. What inhibition mechanism can lead to high state-dependence? The obvious requirement: high affinity to inactivated state and low affinity to resting state, is not sufficient: The higher the affinity to inactivated state, the slower the dissociation must be,
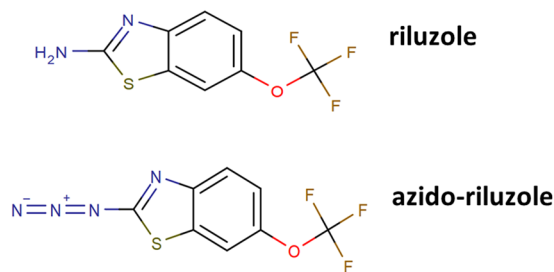
Figure 2. Chemical structure of riluzole and azido-riluzole.

and slow dissociation will necessarily compromise physiological function. In order to achieve sufficiently high state-dependence, the compound must either be able to associate/dissociate particularly rapidly, or it must be able to allow conduction while being bound to the channel. In the case of riluzole, a drug with an exceptionally high state-dependence (see below), we will investigate both possibilities.

Is it at all possible for a drug-bound channel to conduct ions? It is generally assumed, that occupancy of the binding site unavoidably blocks the channel, therefore channel block and modulation cannot be distinguished in electrophysiology experiments. Contrary to this prevalent assumption, it has never been proven that a single inhibitor molecule must fully prevent conduction. In fact, molecular dynamics simulations have raised this very question, as it was discussed by Martin and Corry[13]: "it is not yet clear if the binding of more than one drug is necessary to occlude the pore or prevent channel opening." Furthermore, it has been shown recently that unlike charged inhibitor molecules, neutral compounds did not displace sodium ions at the selectivity filter, but tended to be positioned near the side of the inner vestibule, away from the selectivity filter[14]. This may be especially true to small compounds, like riluzole.

In this study we intended to investigate if non-blocking modulation is at all possible. Are there sodium channel inhibitor compounds that are predominantly blockers, and ones that are predominantly modulators? Could we specifically search for effective modulators which are at the same time weak blockers? These compounds would be expected to cause less adverse effects but more therapeutic effect.

The standard **SSI** and **RFI** protocols are able to assess both resting channel block (seen as the extent of inhibition after the cell has spent sufficient time at negative holding potentials) and modulation (seen as the extent of shift of **SSI** and **RFI** curves) at the same time (Fig. 1). The contribution of non-blocking- and blocking-modulation, however cannot be judged from these protocols alone. We made an attempt to assess the contribution of non-blocking modulation to the inhibition mechanism of riluzole.

Unique Properties of Riluzole

A good candidate for a drug that has a favorable modulation *vs.* block profile is the neuroprotective drug, riluzole (Fig. 2), which has been found to show uncommonly strong state-dependence: strong shift of the **SSI** curve with minimal inhibition of current amplitude at hyperpolarizing membrane potential (Fig. 1). Both in our comparative study of 35 drugs[6], and in a meta-analysis of literature data[15], riluzole was consistently among the compounds with the highest state-dependence (ratios of resting/inactivated state affinities were between 150 to 749). Figure 3 illustrates results from the meta-analysis[15], altogether 194 individual inactivated–resting affinity data pairs are plotted. Measurements of riluzole from four different publications are shown as red symbols. Affinities to resting state ranged between 30 and 426 μM, while inactivated state affinities were between 0.2 and 1.2 μM. We should mention that effective concentrations that inhibited firing in neurons (0.5 to 3.9 μM), or the persistent component of the sodium current (0.55 to 2.2 μM) were in the range of inactivated state affinities[16–20].

In this study we intended to understand the reason for this property: Is it simply due to a higher difference between resting-state and inactivated-state affinities, or can it be due to the fact, that this compound is more of a modulator than a channel blocker? Could one find sodium channel inhibitor (SCI) drugs that are predominantly modulators? If yes, these would be more selective for pathological conditions, and therefore would show less adverse effects.

The problem with separating modulation from block is that in experiments we can only distinguish conducting and non-conducting channels. For example a delayed recovery observed in a standard **RFI** protocol is usually thought to reflect dissociation of the drug, because drug-bound channels are generally considered non-conducting per se. However, if drug binding does not necessarily exclude conduction, delayed recovery could also reflect the gating process itself, without dissociation (recovery itself must be delayed, according to the modulated receptor hypothesis). One way to test this is to eliminate one of the unknowns, the possibility of dynamic association and dissociation of the ligand during experiments. To accomplish this, we used a photoreactive riluzole analog, azido-riluzole (Fig. 2a), which can be induced to bind covalently to the channel by UV illumination.

Photolabeling-Coupled Electrophysiology

The method of photoaffinity labeling (PAL) is conventionally used for target and binding site identification[21–24]. However, the method can also be used to study direct effects of ligands (agonists, antagonists, inhibitors, modulators), when combined with electrophysiology. This allows real-time monitoring of the effect and its reversibility, both with and without photoactivation. Photolabeling-coupled electrophysiology has been used to study the
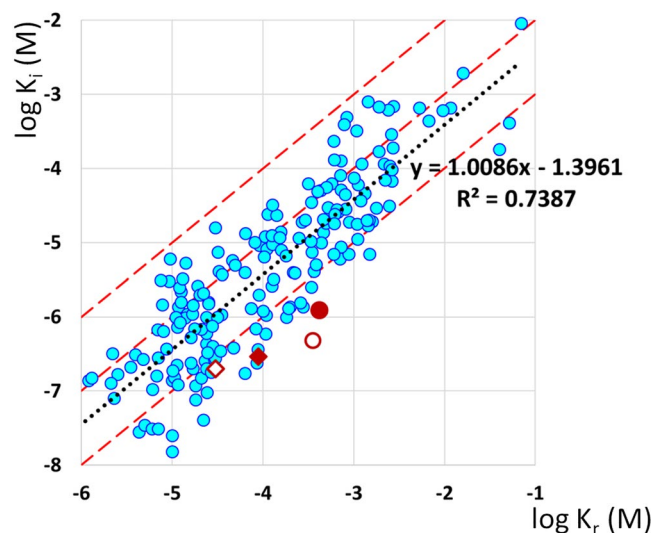
Figure 3. State-dependence of riluzole in comparison with 122 SCI compounds. Data are from Supplement #3 of[15]; excluding Nav1.8-selective compounds. Inactivated affinities are plotted against resting affinities. We collected 194 individual data pairs of 122 compounds from 73 publications. Data were calculated from inhibition at different holding potentials, as described in[40]; corrected and standardized, as described in[15]. Data for riluzole are shown in red: ♦[41], ◇[42], ●[6], o:this study. The black dotted line is the linear regression line, with equation and correlation coefficient (R^2). The average state-dependence, calculated from the y intercept of the linear regression line was 24.8-fold. Red dashed lines indicate $K_r = K_i$; $K_r = 10*K_i$; and $K_r = 100*K_i$. The state-dependence of riluzole was above 100-fold in all studies.

interaction between binding site occupancy and gating, stoichiometry and cooperativity in different ligand-gated ion channels[25–29]. In the case of sodium channels, our motivation was to test, whether the modulation of channel gating kinetics persisted after covalently binding and then washing out the photoreactive inhibitor compound. We reasoned that if modulation still persists after complete washout, then this state-dependent component of inhibition must come from a non-blocking modulation of sodium channels.

When designing a photoreactive sodium channel inhibitor, certain properties of the binding site must be taken into consideration. The binding site is located in the "inner vestibule", which is an aqueous cavity inside the pore region of the channel, surrounded by the S5 and S6 transmembrane segments of all four domains. It is limited by the selectivity filter from the extracellular side, and by the activation gate from the intracellular. Access to the inner vestibule is either through the activation gate during open state (hydrophilic pathway), or through the "fenestrations" directly from the membrane phase (hydrophobic pathway). Most drugs predominantly use the hydrophobic pathway, i.e., they can readily associate even without channel opening. Mutagenesis studies indicate that residues of S6 segments from domains I, III and IV contribute to the binding site[30], the most important being a Phe residue in DIV (F1579 in Nav1.4). Because of these properties of the binding site, there are some strict structural requirements to consider when designing a photoreactive SCI analog: Because the access pathway involves partitioning into the lipid bilayer, lipophilicity of the compound is crucial. There is a strong correlation between lipophilicity (logP) and affinity for SCI compounds, probably because SCI molecules accumulate within the membrane phase[6,15]. In addition, the number of aromatic rings is strongly correlated with onset and offset rates and reversibility[6,31]. Finally, the size of the molecule is also crucial. One reason for the exceptional properties of riluzole might be its size; it has the lowest atom count (20) and van der Waals volume (164 Å^3) among effective SCI compounds[15,31]. For these reasons, attaching one of the most commonly used groups, phenylazide, phenyldiazirine or benzophenone, would have been unadvisable. Fortunately, the aryl-amine group of riluzole can be changed into an aryl-azide, which is the smallest possible modification that produces a photoreactive analog. The azide group still alters important physicochemical properties of the compound, most importantly the charge distribution and lipophilicity, therefore the similarity of the effect of riluzole and azido-riluzole must be investigated. The compound was found to possess stability in the dark, and was highly reactive upon UV irradiation. Intermediates of photo-activated aryl-azides had sufficiently short lifetime (in the ps range)[32], therefore binding should occur before the activated drug leaves the binding site by diffusion.

Results

Inhibition of Na$_V$1.4 sodium channels by riluzole. The effect of 10 and 100 μM riluzole on the gating equilibrium and kinetics was studied using the steady-state inactivation (**SSI**) the recovery from inactivation (**RFI**) and the state-dependent onset (**SDO**) protocols. All three protocols were used before, during and after drug perfusion, the full experiment lasted 12 to 20 minutes. Although riluzole concentrations are higher than what was found effective in decreasing firing rate, we sought to understand the mechanism by using concentrations that could ensure fast association and high occupancy of binding sites.

In the **SSI** protocol the membrane potential was set for 10 ms to pre-pulse potentials between −130 mV and −20 mV in 5 mV increments, which was followed by a 10 ms test pulse to −10 mV, in which the availability of the channel population was assessed (Fig. 1). The relatively short pre-pulse potential, which was chosen to exclude intermediate inactivation, was nevertheless enough to reach equilibrium at 100 μM riluzole. Data points were fit with the Boltzmann function, from which the half inactivation voltage ($V_{1/2}$) values were determined. In control experiments the $V_{1/2}$ was 56.3 ± 3.76 mV, which was shifted to the hyperpolarized direction by $−27.5 \pm 3.95$ mV by 100 μM riluzole (Fig. 4b). The $V_{1/2}$ value did not always recover to its original value upon washout, because – as it is well documented in the literature – it tends to undergo a spontaneous left shift during whole-cell recording. For this reason, the shift caused by drugs may be somewhat overestimated.

This drawback, however was absent in the **RFI** protocol, where the time constant of recovery always faithfully regained its control value upon washout. The **RFI** protocol consisted of two equal 10 ms depolarizations to −10 mV, separated by a hyperpolarizing gap (−130 mV) with logarithmically increasing duration (multiplied by 1.5) between 0.1 ms and 65.7 ms (Fig. 1). In the presence of 100 μM riluzole the time constant was increased 6.33-fold (range: 5.27- to 9.65-fold): while drug-free channels recovered from inactivated state with the time constant of 0.49 ± 0.09 ms, in the presence of riluzole the time constant was 2.97 ± 0.50 ms ($p = 4*10^{-7}$, $n = 7$) (time constants are for the exponential on the third power, see Methods). At the same time, the decrease in amplitude was minimal, it decreased to $87.5 \pm 4.78\%$ of the original amplitude ($p = 0.03$). The average and SEM of fitted curves are shown in Fig. 4.

Inhibition was strongly state-dependent, therefore we intended to investigate the onset of inhibition upon depolarization. The **SDO** protocol consisted of two depolarizations (from −130 mV to −10 mV), separated by a 2 ms hyperpolarization. The length of the first depolarization was increased logarithmically by a factor of 2 from 0.5 ms to 512 ms. The second pulse served to measure availability. Under control conditions we observed only a minor decrease in amplitude due to incomplete recovery from fast inactivation, and intermediate inactivation. In the presence of 10 μM riluzole, however, the amplitude rapidly decreased with a time constant of 4.89 ± 0.53 ms ($n = 8$), due to either fast association, or a conformational rearrangement of the ligand-channel complex during depolarization (Fig. 4a, right column). In the presence of 100 μM riluzole (Fig. 4b, right column) the state-dependent onset of inhibition became so fast ($\tau = 0.35 \pm 0.056$ ms, $n = 7$) that the first segment of the onset curve was already missed at the shortest, 0.5 ms interval. (In Fig. 4a to d curves were normalized to the control amplitude. In Fig. 4e and in the insets of Fig. 4d curves were normalized to their own maxima, i.e., to the maxima in the presence of the treatment. In the case when the amplitude was already reduced even after the shortest pulse, we normalized to the maximal amplitude of currents evoked by the preceding **SSI** protocol.)

In order to monitor the onset and offset of the effect, we used a three-pulse train (**3PT**) protocol (Fig. 5), which was designed to indicate changes both in the gating kinetics and gating equilibrium. The first depolarizing pulse measured resting inhibition, because it was evoked from a prolonged hyperpolarized membrane potential (263 ms at −130 mV). The second was designed to indicate changes in the recovery kinetics, and it followed the first one after a 5 ms hyperpolarizing gap (−130 mV). This duration enables drug-free channels to recover completely from inactivation ($99 \pm 0.004\%$), while in the presence of 100 μM riluzole the recovery was incomplete ($57.7 \pm 8.7\%$). A drug that modulates recovery kinetics, should show a selective inhibition of the 2nd pulse as compared to the 1st one. Finally, the 3rd pulse was designed to indicate changes in gating equilibrium. Before this 3rd pulse the holding potential was elevated to the approximate $V_{1/2}$ value of the **SSI** curve (set individually for each cell, ranging between −75 and −50 mV) for 50 ms. The amplitude of this 3rd pulse was a very sensitive indicator of changes in the voltage-dependence of inactivation. Three-pulse trains were evoked every 333 ms. Using this protocol, we could measure the three important properties (resting inhibition, modulation of gating kinetics, modulation of gating equilibrium) of the effect of SCIs in parallel and with reasonable time resolution. Higher frequency would not improve time resolution, because it was limited by the rate of solution exchange (~1–2 s). The time course of the onset and offset of inhibition is shown in Fig. 5 for the three pulses in parallel. The ratios of 2nd/1st and 3rd/1st pulse-evoked amplitudes are even more informative regarding the extent of modulation; they indicate the drug's potency for affecting gating kinetics and gating equilibrium, respectively. We show these ratios, calculated from the average traces for 100 μM and 10 μM riluzole, as well as for azido-riluzole with and without UV irradiation in Fig. 5e. Note that riluzole was much more effective as a modulator than as a resting state blocker.

This was clearly observable even at 10 μM concentration, where the onset rate was lower, and the inhibition somewhat smaller, but the considerable modulation (see 2nd/1st and 3rd/1st pulse-evoked amplitude ratios in Fig. 5a,e) as compared to the minimal resting block (see the minimal effect on the 1st pulse-evoked current) shows the peculiar nature of inhibition by riluzole.

Application of UV irradiation for 180 s did not change the inhibition by riluzole in any of the three protocols. Similarly, UV irradiation did not alter control values (data not shown).

Inhibition by azido-riluzole. Without UV irradiation 100 μM azido-riluzole caused a weaker shift in **SSI**, **RFI**, and **SDO** curves than riluzole, although the resting state inhibition was similar (Fig. 4). This indicates that it is equipotent in inhibiting resting conformation, but shows less state-dependence than riluzole. The reason for this may be its slower association/dissociation kinetics, or that it is a less effective modulator. Slower association kinetics can be observed in the **SDO** protocol (Fig. 4c), and also in the **3PT** protocol (Fig. 5c), where the onset and offset of inhibition were slower. This was expected, because access to the binding site should be faster in the case of the less polar riluzole (the polar surface area of riluzole and azido-riluzole are 48.14 Å² and 51.55 Å², respectively) which also has a more uniform charge distribution. Neither compounds have net positive charge, the pKa of riluzole is 4.57, while azido-riluzole cannot be protonated. Interestingly, lipophilicity of azido-riluzole is predicted to be even higher than that of riluzole: calculated logP values are 4.65 and 3.40, respectively. In terms of modulation of the gating equilibrium, 100 μM azido-riluzole was roughly equi-effective with 10 μM riluzole, as seen by the shift of the **SSI** curve (Fig. 4b and c), and the 3rd/1st pulse evoked current amplitude ratio (Fig. 5e). The $V_{1/2}$ was
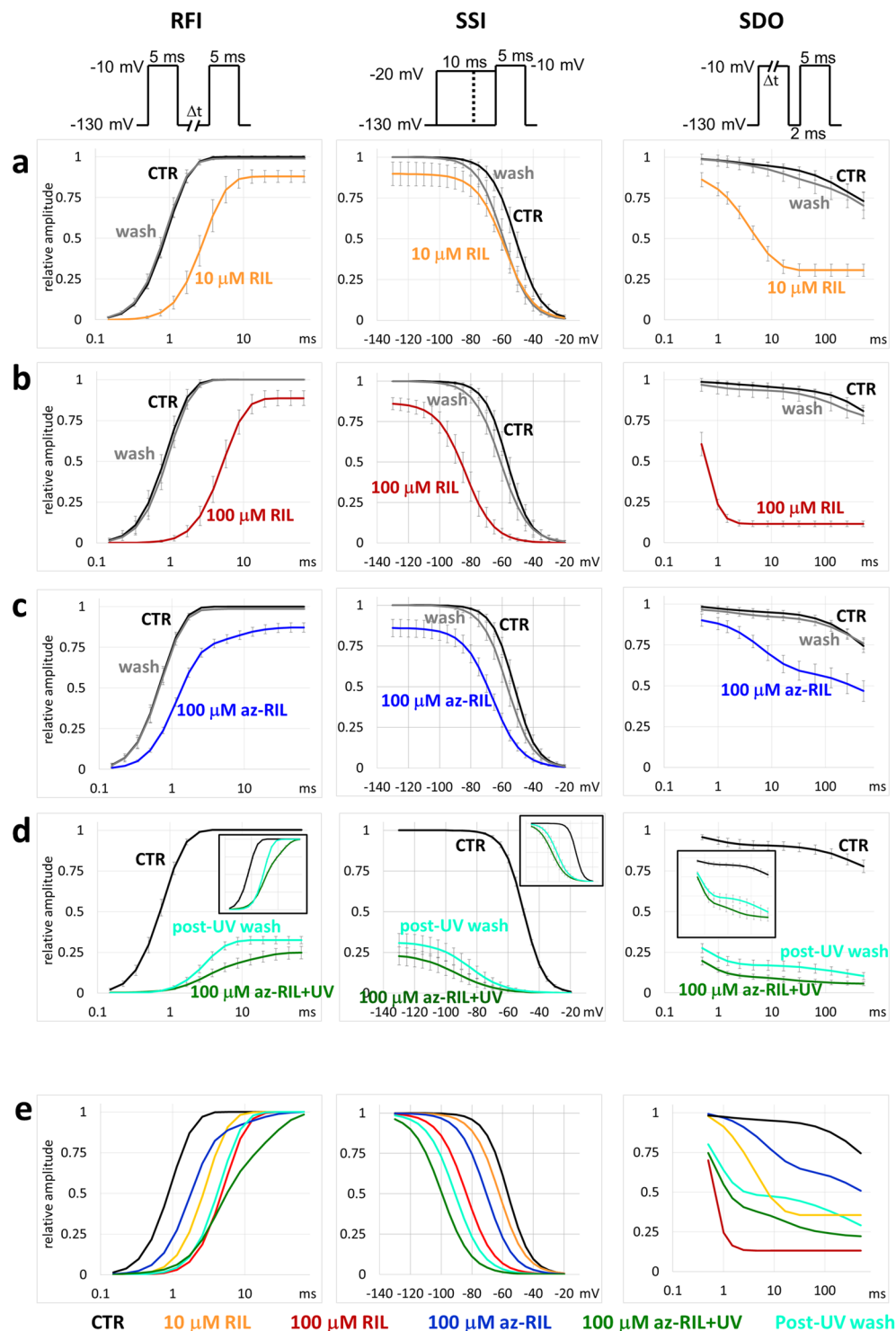
Figure 4. The effect of 10 and 100 μM riluzole and 100 μM azido-riluzole in the **RFI**, **SSI** and **SDO** protocols. Black, colored and gray lines indicate control, drug and washout, respectively. (**a**) 10 μM riluzole. (**b**) 100 μM riluzole. (**c**) 100 μM azido-riluzole. (**d**) 100 μM azido-riluzole during UV-irradiation, and after washout. Turquoise lines indicate washout after azido-riluzole perfusion and UV-irradiation. Insets show curves normalized to their own maxima. Averaging was done as described in Methods. (**e**) Comparison of the effects of all five treatments. All curves were normalized to their own maxima.

shifted to the hyperpolarized direction by -14.0 ± 2.21 mV (Fig. 4c). In terms of modulation of gating kinetics, azido-riluzole had even weaker effect than 10 μM riluzole, as seen in the **3PT** protocol, where there was hardly any difference between the inhibition of the 1st and 2nd pulse-evoked currents (Fig. 5c and e). In addition, **RFI** curves were only moderately shifted: the fast time constant of recovery increased only 1.6-fold (range: 1.33- to 2.36-fold;
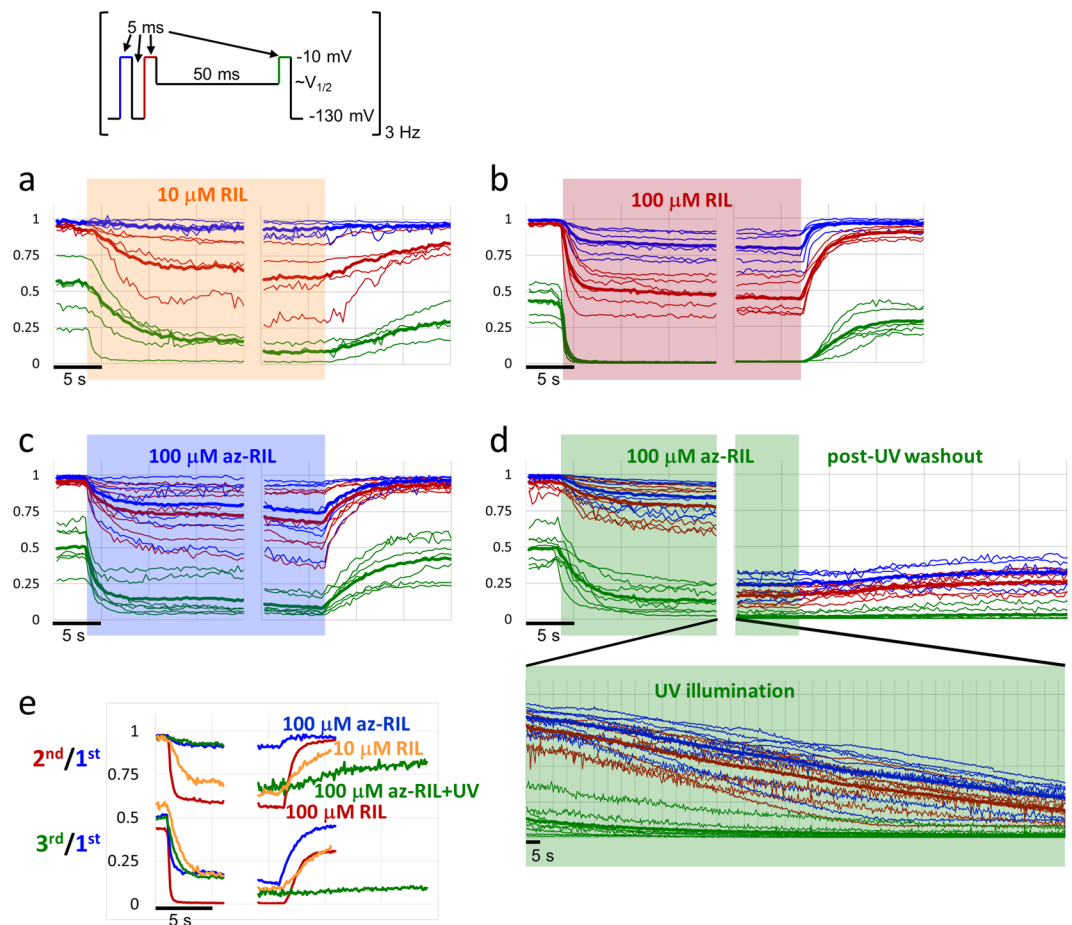
Figure 5. Onset and offset of drug effects in the **3PT** protocol. Plots of peak amplitudes for the 1st, 2nd, and 3rd pulse-evoked currents are shown in blue, red and green lines, respectively. Thin lines show measurements from individual cells, thick lines show averages. Recordings from individual cells were aligned to the moment of wash-in and wash-out for comparability, with 0 to 767 s of recording not shown between the onset and offset. Ten control trains (3.3 s) are shown before drug applications, and the last 20 trains (6.6 s) of drug application before wash-out. (**a**) 100 μM riluzole, (**b**) 10 μM riluzole, (**c**) 100 μM azido-riluzole, (**d**) 100 μM azido-riluzole with UV irradiation (shown on a contracted time scale below onset and offset). (**e**) Plot of $2^{nd}/1^{st}$ pulse-evoked (upper curves) and $3^{rd}/1^{st}$ pulse-evoked (lower curves) amplitude ratios for the onset and offset of: 10 μM riluzole (yellow lines), 100 μM riluzole (red lines), 100 μM azido-riluzole (blue lines), and 100 μM azido-riluzole with ~3 min UV irradiation (green lines) between onset and offset.

p = 1*10^{-4}, n = 7); and **SDO** curves showed a slower onset (the fast time constant was 7.90 ± 1.34 ms, n = 6) and less inhibition than in the case of even 10 μM riluzole (compare Fig. 4b,c and e). In addition to the delayed fast component, a second, slow component appeared, the time constant of which was 7.37 ± 1.23 ms (range: 4.65 to 14.2 ms), and its contribution to the amplitude was 17.6 ± 3.8% (range: 11.1 to 35.2%) (Fig. 4c).

The effect of UV-illumination in the presence of azido-riluzole.
We applied a single 180 s UV irradiation in the presence of 100 μM azido-riluzole while running the **3PT** protocol, which resulted in a slow continuous decrease of 1st pulse evoked sodium current amplitudes, to 25.3 ± 3.6% of its initial value (Fig. 5d). The slow decay depended on the presence of UV light: when illumination was suspended, the decay was also temporarily halted. The inhibition recovered to 32.5 ± 3.8% of the initial value upon washout, the roughly 7% difference probably reflects dissociation and washout of unactivated azido-riluzole. By the end of azido-riluzole treatment, UV irradiation and washout, thus 67.5% of the control current amplitude was irreversibly inhibited by the covalently bound azido-riluzole. The inhibition persisted throughout the rest of the experiment, for up to 20 minutes post-UV exposure. Currents evoked by 2nd pulses were irreversibly reduced to 25.5 ± 2.8%, while currents evoked by the 3rd pulse to 2.78 ± 1.62% of the pre-UV amplitude.

One crucial question was, whether covalently bound azido-riluzole causes only channel block, or also modulation. In this situation when unbound azido-riluzole had already been washed out, delayed recovery cannot reflect the process of dissociation, only modulated gating. Similarly, a shifted **SSI** curve cannot be caused by state-dependent affinity, because no association and dissociation can occur, therefore the only explanation must be modulation. If one can see signs of modulation by covalently bound inhibitor, it proves that non-blocking

modulation is possible, and therefore, it might be responsible for a fraction of inhibition in the case of non-covalently bound riluzole as well. This could in part explain the peculiar behavior of riluzole (small resting state inhibition with strong modulation).

As it can be seen in Fig. 4d, the remaining component of the sodium current was strongly modulated by the covalently bound inhibitor (there was no perfused inhibitor present). The extent of modulation was close to the values observed in the presence of 100 μM riluzole. The **SSI** curve was shifted by -42.8 ± 4.33 mV post-UV in the presence of 100 μM azido-riluzole, and was still shifted by-34.3 ± 6.93 mV after washout. Recovery kinetics was clearly bi-exponential in the presence of azido-riluzole, the fast component increased 3.99-fold (range: 2.46- to 6.14-fold; $p = 7.8*10^{-4}$, $n = 8$), and a slow component emerged with a time constant of 12.6 ± 1.31 ms (range: 7.2 to 17.7 ms), contributing $52.1 \pm 3.18\%$ to the amplitude (range: 38.7 to 62.4%). After washing out unactivated azido-riluzole, the time course of recovery again could be reasonably well fitted with a single exponential component (on the third power), which probably indicates that the slow component was due to azido-riluzole dissociation. The time constant after washout was 4.48-fold higher than the time constant of control curves (range: 2.44 to 7.57-fold change; $p = 1.7*10^{-5}$, $n = 8$). Unexpectedly, the shape of the **SDO** curve indicated that the remaining component of the current did have a definite fast onset kinetics even after UV irradiation and complete washout, that was similar to the one observed in the presence of 100 μM riluzole, in spite of the fact that no association was possible any more. The fast time constant of the post-UV **SDO** curve was 0.68 ± 0.09 ms, and it contributed $51.3 \pm 2.4\%$ to the amplitude. It must reflect a conformational rearrangement that occurred upon each depolarization. The slow time constant contributes less to the amplitude ($34.0 \pm 5.6\%$), and it most probably reflects slow inactivation of the channel.

Note that azido-riluzole shifted **RFI** curves in a way, that – just as in the case of 100 μM riluzole, see Fig. 4b and d – inhibition was close to 100% at gap durations < 1 ms. This indicates close to full occupancy of binding sites, nevertheless, $32.5 \pm 3.8\%$ of the control current was able to flow through channels with covalently bound inhibitors. Binding to areas of the channel other than the primary binding site (known as the "local anesthetic receptor") might have occurred, however, this could not account for modulation. Mutation of the key residue of the primary binding site, Phe1579 abolished modulation[33], similarly to what have been observed in other laboratories, where this mutation selectively abolished use-dependent inhibition[34], the shift of **SSI** curves[35] as well as the effect of SCIs on voltage sensor movement[35,36]. Similarly, in the **SSI** curves inhibition was close to 100% at membrane potentials > -50 mV. Full inhibition can only be caused by full occupancy of binding sites, which implies that at hyperpolarized potentials conduction occurred in spite of the presence of a covalently bound inhibitor at the binding site.

Discussion

We have performed a photolabeling-coupled patch-clamp study on hNa$_V$1.4 sodium channels, and the effect of a novel photoactive inhibitor, azido-riluzole. Our method allowed not only to monitor the extent of inhibition during the process of photolabeling, but also to assess the contribution of channel block and channel modulation.

Riluzole is unique among SCIs because of its high state-dependence, and its ability to cause strongly shifted **SSI** and **RFI** curves, while causing minimal resting state inhibition. These properties seem beneficial, since they promote a strong selectivity depending on the health of the tissue or individual cells. The reason for such properties may be that the compound is predominantly a modulator and only a weak blocker, or it may be due to an extremely fast onset/offset kinetics. We hypothesize that both the ability to cause non-blocking modulation, and the ability to access the binding site extra fast, may be due to special physicochemical properties of riluzole: small volume, high lipophilicity and neutrality. Our aim was to learn more of the mechanism of sodium channel inhibition by riluzole, most importantly we wanted to test if modulation might exist without channel block.

In order to answer this question we needed to eliminate the unknown of association/dissociation dynamics of the ligand from the experiments. Interpretation of kinetic experiments is complicated by the simultaneous and mutually interacting processes of channel gating and drug binding/unbinding. If one can make experiments with covalently bound inhibitor molecules, this ambiguity can be excluded.

We performed experiments with the photoactive analog of riluzole, azido-riluzole. The compound could be activated by UV irradiation at 310 nm wavelength, which –at least for the 180 s duration we used in our experiments – did not cause noticeable damage to the cells. This indicates that azido-riluzole could be used in *in vivo* experiments as well. We demonstrated that UV illumination increased its potency (as if it was applied at a higher concentration), and made it to be irreversible on the time scale of an average electrophysiology experiment. Upon UV irradiation a virtual increase in affinity occurs, which allows this compound to be used in experiments where localized effects of sodium channel inhibition are to be studied.

The compound azido-riluzole did not qualify as the exact replica of riluzole, with the only difference of being photoactive. The necessary changes in chemical composition caused it to have less affinity, furthermore it showed more resting inhibition and less state-dependent modulation as compared to riluzole. Nevertheless, it still maintained a definite modulatory component of inhibition. The principal question was, if it would still maintain its ability to modulate after having bound covalently to its binding site within the channel.

Significantly, after photoactivation, covalent binding to the channel, and subsequent wash-out of the unbound fraction, the bound fraction of azido-riluzole was still able to exert a modulatory effect that resembled the modulation caused by 100 μM riluzole. The effect could be due to binding to distinct binding sites within individual channels, i.e., blocking the pore by binding to the conventional local anesthetic binding site and causing modulation by binding to a novel site. Our experiments with mutant channels, where the key phenylalanine residue of the local anesthetic binding site has been changed to alanine (F1579A) argue against this possibility. In F1579A mutant channels not only the affinity of riluzole was decreased, but the modulation has also been practically abolished[33]. This is best judged from the **RFI** protocol, where apparent affinity (calculated from the extent of inhibition) decreased radically (61-fold) at 1 ms interpulse interval, but only 2- to 4-fold at >10 ms interpulse intervals.

We can conclude that non-blocking modulatory effect on sodium channels is possible, and it can be part of the explanation for the extraordinary properties of inhibition caused by the parent molecule, riluzole as well. We hypothesize that this special kind of inhibition is due to the special physicochemical properties of riluzole, namely its small volume, neutrality and lipophilicity. This hypothesis opens the way to the search for other non-blocking modulatory SCI drugs, which are expected to have stronger therapeutic and less severe adverse effects.

Methods

Cloning and stable cell line generation.
To maximize recombinant sodium channel expression, the coding sequence of the rat $Na_V1.4$ sodium channel was inserted into a modified pBluescript KS (Stratagene, La Jolla, CA) vector (pCaggs IgG-Fc) capable to recombine with the murine Rosa26 BAC[37]. Briefly, $Na_V1.4$ was inserted into the vector at *AscI* sites under the control of the Caggs promoter. Recombination to the *Rosa26* BAC was carried out by Recombineering[38,39]. Original BAC clone RP24-85I15 was derived from the BACPAC Resources Center (Children's Hospital Oakland Research Institute). $Na_V1.4$ BAC was transfected into CHO DUKX B11 (ATCC CRL-9096) suspension cells by Fugene HD (Promega, Fitchburg, WI) transfection reagent according to the manufacturer's recommendations. Cell clones with stable vector DNA integration were selected by the addition of G418 antibiotic to the culture media (400 mg/ml) for 14 days.

Cell culture and expression of recombinant sodium channels.
CHO cells were maintained in Iscove's Modified Dulbecco's Medium with 25 mM HEPES and L-Glutamine (Lonza, Basel, Switzerland) supplemented with 10% v/v fetal calf serum, 200 mM L-glutamine, 100 U/ml of penicillin/Streptomycin, 0.5 mg/mL Geneticin(Life Technologies, Carlsbad, CA) and 2% ProHT Supplement (Lonza). Cells were plated onto 35 mm petri dishes and cultured for 24–36 hours. Prior to experiments cells were dissociated from the dish with trypsin-EDTA, centrifuged and suspended into the extracellular solution.

Materials
All chemicals were obtained from Sigma-Aldrich. Azido-riluzole was synthesized by SONEAS Research Ltd. Budapest, Hungary

UV photoactivation.
The recording chamber of a Port-a-Patch system (Nanion, Munich, Germany) was customized to accommodate a 400 μm diameter quartz optic fiber, which was placed 3–4 mm above the recorded cell. The original perfusion manifold was replaced by a custom manifold positioned to the side of the recording chamber opposite to the waste removal. Solution exchange was complete within 1–2 s. UV light was applied for 180 s, using a 310 nm fiber coupled Mightex FCS-0310-000 LED (Mightex, Pleasanton, CA), with 40 μW intensity.

Electrophysiology.
Whole-cell currents were recorded from cells voltage clamped at −130 mV using an EPC10 plus amplifier, and the PatchMaster software (HEKA Electronic, Lambrecht, Germany). During cell catching, sealing, and whole-cell formation, the PatchControl software (Nanion) commanded the amplifier and the pressure control unit. Currents were filtered at 10 kHz, and digitized at 20 kHz. The intracellular solution contained (mM): 50 CsCl, 10 NaCl, 60 CsF, 20 EGTA, 10 HEPES; pH 7.2 (adjusted with 1 M CsOH). The resistance of borosilicate chips was 2.0–3.5 MΩ. Cells were continuously perfused with extracellular solution containing (mM): 140 NaCl, 4 KCl, 1 MgCl$_2$, 2 CaCl$_2$, 5 D-Glucose and 10 HEPES; pH 7.4 (adjusted with 1 M NaOH).

Data analysis.
Curve fitting was done in Microsoft Excel, using the Solver Add-in. Steady-state inactivation (**SSI**) curves were fitted using the Boltzmann function:

$$I = I_{max}/\{1 + \exp[(V_p - V_{1/2})/-k]\},$$

where V_p is the pre-pulse potential, $V_{1/2}$ is the voltage where the curve reaches its midpoint, and k is the slope factor. Recovery from inactivation (**RFI**) data were fitted by exponential function. We noticed that a simple exponential function did not adequately fit data points, the fit much improved when the exponential equation was on the second power, and further improved on the third power:

$$I = A^*\left[1 - \exp\left(-t_{ip}/\tau\right)\right]^3,$$

where A is the amplitude, and t_{ip} is the duration of the interpulse interval. The time constant of best fit equations changes with the power, for example the same control recovery curve was fitted with $\tau = 1.09$ ms (1st power), $\tau = 0.62$ ms (2nd power), and $\tau = 0.48$ ms (3rd power). In order to keep time constants comparable we fixed the exponent at the value of 3 for all curves during fitting. In the presence of azido-riluzole adequate fitting required a second exponential component, therefore these data were fit with the following equation:

$$I = A_1^*\left[1 - \exp\left(-t_{ip}/\tau_1\right)\right]^3 + A_2^*\left[1 - \exp\left(-t_{ip}/\tau_2\right)\right].$$

State-dependent onset (**SDO**) data were fitted with either single or double exponential functions:

$$I = A_1^*\exp\left(-t_p/\tau_1\right) + A_2^*\exp\left(-t_p/\tau_2\right),$$

where A_1 and A_2 are the relative amplitudes of the two components, and t_p is the duration of the pulse.

Averaging was not done by calculating the mean value of data points across individual cells, because that would have resulted in an erroneously decreased slope of averaged curves. Instead, for each individual cell data points were fitted separately, and curves were reconstructed from the averaged parameters of equations (time

constants and amplitudes in the case of **RFI** curves, $V_{1/2}$ values and slope factors in the case of **SSI** curves). Error bars show SEM for original data points. All data are presented as mean $\pm$ SEM for the indicated number of experiments (n). Significance levels were calculated using paired Student's t test. Chemical property prediction and calculation was done using JChem for Excel 15.4 software from ChemAxon (Budapest, Hungary) (http://www.chemaxon.com).

Data availability.   The datasets generated and analyzed during the current study are available from the corresponding author on reasonable request.

References

1. Eijkelkamp, N. *et al*. Neurological perspectives on voltage-gated sodium channels. *Brain* **135**, 2585–2612 (2012).
2. Tarnawa, I., Bölcskei, H. & Kocsis, P. Blockers of voltage-gated sodium channels for the treatment of central nervous system diseases. *Recent Patents CNS Drug Discov.* **2**, 57–78 (2007).
3. Payandeh, J. & Minor, D. L. Bacterial Voltage-Gated Sodium Channels (BacNaVs) from the Soil, Sea, and Salt Lakes Enlighten Molecular Mechanisms of Electrical Signaling and Pharmacology in the Brain and Heart. *J. Mol. Biol.* **427**, 3–30 (2015).
4. Bagal, S. K., Marron, B. E., Owen, R. M., Storer, R. I. & Swain, N. A. Voltage gated sodium channels as drug discovery targets. *Channels Austin Tex* **9**, 360–366 (2015).
5. England, S. & de Groot, M. J. Subtype-selective targeting of voltage-gated sodium channels. *Br. J. Pharmacol.* **158**, 1413–1425 (2009).
6. Lenkey, N. *et al*. Classification of drugs based on properties of sodium channel inhibition: a comparative automated patch-clamp study. *PLoS One* **5**, e15568 (2010).
7. Hille, B. Local anesthetics: hydrophilic and hydrophobic pathways for the drug-receptor reaction. *J. Gen. Physiol.* **69**, 497–515 (1977).
8. Hondeghem, L. M. & Katzung, B. G. Time- and voltage-dependent interactions of antiarrhythmic drugs with cardiac sodium channels. *Biochim. Biophys. Acta* **472**, 373–398 (1977).
9. Starmer, C. F., Grant, A. O. & Strauss, H. C. Mechanisms of use-dependent block of sodium channels in excitable membranes by local anesthetics. *Biophys. J.* **46**, 15–27 (1984).
10. Morris, C. E. & Joos, B. Nav Channels in Damaged Membranes. *Curr. Top. Membr.* **78**, 561–597 (2016).
11. Fischer, B. D., Ho, C., Kuzin, I., Bottaro, A. & O'Leary, M. E. Chronic exposure to tumor necrosis factor *in vivo* induces hyperalgesia, upregulates sodium channel gene expression and alters the cellular electrophysiology of dorsal root ganglion neurons. *Neurosci. Lett.* **653**, 195–201 (2017).
12. Barker, B. S. *et al*. Pro-excitatory alterations in sodium channel activity facilitate subiculum neuron hyperexcitability in temporal lobe epilepsy. *Neurobiol. Dis.* **108**, 183–194 (2017).
13. Martin, L. J. & Corry, B. Locating the route of entry and binding sites of benzocaine and phenytoin in a bacterial voltage gated sodium channel. *PLoS Comput. Biol.* **10**, e1003688 (2014).
14. Buyan, A., Sun, D. & Corry, B. Protonation state of inhibitors determines interaction sites within voltage-gated sodium channels. *Proc. Natl. Acad. Sci. USA* **115**, E3135–E3144 (2018).
15. Lenkey, N., Karoly, R., Epresi, N., Vizi, E. & Mike, A. Binding of sodium channel inhibitors to hyperpolarized and depolarized conformations of the channel. *Neuropharmacology* **60**, 191–200 (2011).
16. Kuo, J. J., Lee, R. H., Zhang, L. & Heckman, C. J. Essential role of the persistent sodium current in spike initiation during slowly rising inputs in mouse spinal neurones. *J. Physiol.* **574**, 819–834 (2006).
17. Cho, J.-H., Choi, I.-S., Lee, S.-H., Lee, M.-G. & Jang, I.-S. Contribution of persistent sodium currents to the excitability of tonic firing substantia gelatinosa neurons of the rat. *Neurosci. Lett.* **591**, 192–196 (2015).
18. Centonze, D. *et al*. Electrophysiology of the neuroprotective agent riluzole on striatal spiny neurons. *Neuropharmacology* **37**, 1063–1070 (1998).
19. Spadoni, F. *et al*. Lamotrigine derivatives and riluzole inhibit INa,P in cortical neurons. *Neuroreport* **13**, 1167–1170 (2002).
20. Ptak, K. Sodium Currents in Medullary Neurons Isolated from the Pre-Botzinger Complex Region. *J. Neurosci.* **25**, 5159–5170 (2005).
21. Catterall, W. A. Finding Channels. *J. Biol. Chem.* **290**, 28357–28373 (2015).
22. Dormán, G. & Prestwich, G. D. Using photolabile ligands in drug discovery and development. *Trends Biotechnol.* **18**, 64–77 (2000).
23. Smith, E. & Collins, I. Photoaffinity labeling in target- and binding-site identification. *Future Med. Chem.* **7**, 159–83 (2015).
24. Woll, K. A., Dailey, W. P., Brannigan, G. & Eckenhoff, R. G. Shedding Light on Anesthetic Mechanisms: Application of Photoaffinity Ligands. *Anesth. Analg.* **123**, 1253–1262 (2016).
25. Bhargava, Y., Rettinger, J. & Mourot, A. Allosteric nature of P2X receptor activation probed by photoaffinity labelling: Binding-gating of P2X receptors. *Br. J. Pharmacol.* **167**, 1301–1310 (2012).
26. Forman, S. A., Zhou, Q. L. & Stewart, D. S. Photoactivated 3-azioctanol irreversibly desensitizes muscle nicotinic ACh receptors via interactions at alphaE262. *Biochemistry (Mosc.)* **46**, 11911–11918 (2007).
27. Mortensen, M. *et al*. Photo-antagonism of the GABAA receptor. *Nat. Commun.* **5**, (2014).
28. Ruiz, M. L. & Karpen, J. W. Single cyclic nucleotide-gated channels locked in different ligand-bound states. *Nature* **389**, 389–392 (1997).
29. Zhong, H., Rüsch, D. & Forman, S. A. Photo-activated azi-etomidate, a general anesthetic photolabel, irreversibly enhances gating and desensitization of gamma-aminobutyric acid type A receptors. *Anesthesiology* **108**, 103–112 (2008).
30. Mike, A. & Lukacs, P. The enigmatic drug binding site for sodium channel inhibitors. *Curr. Mol. Pharmacol.* **3**, 129–144 (2010).
31. Lazar, A., Lenkey, N., Pesti, K., Fodor, L. & Mike, A. Different pH-sensitivity patterns of 30 sodium channel inhibitors suggest chemically different pools along the access pathway. *Front. Pharmacol.* **6**, 210 (2015).
32. McCulla, R. D., Burdzinski, G. & Platz, M. S. Ultrafast study of the photochemistry of 2-azidonitrobenzene. *Org. Lett.* **8**, 1637–1640 (2006).
33. Szabo, A. K. *et al*. Non-blocking modulation as the major mechanism of sodium channel inhibition by riluzole. https://doi.org/10.1101/228569 (2017).
34. Ragsdale, D. S., McPhee, J. C., Scheuer, T. & Catterall, W. A. Molecular determinants of state-dependent block of Na+ channels by local anesthetics. *Science* **265**, 1724–1728 (1994).
35. Hanck, D. A. *et al*. Using Lidocaine and Benzocaine to Link Sodium Channel Molecular Conformations to State-Dependent Antiarrhythmic Drug Affinity. *Circ. Res.* **105**, 492–499 (2009).
36. Muroi, Y. & Chanda, B. Local anesthetics disrupt energetic coupling between the voltage-sensing segments of a sodium channel. *J. Gen. Physiol.* **133**, 1–15 (2009).
37. Zboray, K. *et al*. Heterologous protein production using euchromatin-containing expression vectors in mammalian cells. *Nucleic Acids Res. gkv475*. https://doi.org/10.1093/nar/gkv475 (2015).
38. Zhang, Y., Buchholz, F., Muyrers, J. P. & Stewart, A. F. A new logic for DNA engineering using recombination in Escherichia coli. *Nat. Genet.* **20**, 123–8 (1998).

39. Muyrers, J. P., Zhang, Y., Testa, G. & Stewart, A. F. Rapid modification of bacterial artificial chromosomes by ET-recombination. *Nucleic Acids Res.* **27**, 1555–7 (1999).
40. Bean, B. P., Cohen, C. J. & Tsien, R. W. Lidocaine block of cardiac sodium channels. *J. Gen. Physiol.* **81**, 613–642 (1983).
41. Benoit, E. & Escande, D. Riluzole specifically blocks inactivated Na channels in myelinated nerve fibre. *Pflüg. Arch. Eur. J. Physiol.* **419**, 603–609 (1991).
42. Hebert, T., Drapeau, P., Pradier, L. & Dunn, R. J. Block of the rat brain IIA sodium channel alpha subunit by the neuroprotective drug riluzole. *Mol. Pharmacol.* **45**, 1055–1060 (1994).

Acknowledgements

Author Contributions

P.L., E.C., L.N., A.M.-C. and A.M. conceived the experiments, P.L., M.C.F., L.V. and B.B.-K. conducted the experiments, P.L., M.C.F. and A.M. analyzed the data, P.L., A.M.-C. and A.M. wrote the manuscript. All authors have read and approved the manuscript.

Additional Information

Competing Interests: The authors declare no competing interests.

Publisher's note: Springer Nature remains neutral with regard to jurisdictional claims in published maps and institutional affiliations.